J. Chem. Sci. (2019)131:89
https://doi.org/10.1007/s12039-019-1668-8

REGULAR ARTICLE

Special Issue on Materials Chemistry

Future demands for high field MRI diagnostic

ANURAG GAUTAM[a,*], PRAGYA KOMAL[b] and RAM SEVAK SINGH[a]
[a]School of Science, O. P. Jindal University, Raigarh 496001, Chhattisgarh, India
[b]Department of Biology, Birla Institute of Technology and Science, Pilani-Hyderabad Campus, Jawaharnagar, Shamirpet Mandal, Hyderabad 500078, Telangana, India
E-mail: ganurag13@gmail.com

MS received 31 March 2019; revised 13 May 2019; accepted 15 May 2019

Abstract. In the near future there would be a need for a high field MRI contrast agent for the MRI diagnostic due to the several disadvantages of Gd-based complexes, such as short circulation time and decrease in efficiency at high magnetic field i.e., greater than 3 T. The lanthanide-based nanoparticle can be an alternative to these complexes due to a high density of metal ions per unit of contrast agent. The high density of the metal ions will enable the MR signal shortening usually, at lower concentrations compared to chelates that typically are used at micro-molar concentrations. Additionally, the nanoparticles would retain their relaxivity efficiency at high magnetic field greater than 3 T.

Keywords. MRI; nanoparticles; magnetic field; relaxivity.

1. Introduction

Nanoparticle-based (NP-based) imaging is currently advancing rapidly for biomedical application such as diagnostic imaging and cancer therapy.[1–23] The major challenge to improve cancer therapy is the detection at early stages when the cancer is still confined to the site of its origin, which could facilitate a more favorable outcome.[2] Magnetic resonance imaging (MRI) is a powerful non-invasive diagnosis technique widely applied for clinical imaging. MRI has a submillimeter spatial resolution, allows whole (human) body scans, and provides details of many diseases.[5–25] As MR image resolution increases with the strength of the magnetic field, high magnetic fields (e.g., 7 T or higher) are used for pre-clinical animal imaging while lower fields ($\leq$3 T) are used for humans. The signal intensity in MRI depends on the proton density and on the T_1 and T_2 relaxation times of the water protons. As the water density is similar for various soft tissues, the differences in the relaxation times are used to provide contrast. However, the differences are often not sufficiently large to allow visible contrast between tumor and normal tissue. Therefore, the tumor contrast must be further improved, by the administration of a contrast agent (CA). The CAs are typically characterized as the enhancement in the T_1 – the longitudinal (spin-lattice) and T_2 – transverse (spin-spin) relaxation rate of the nearby water proton. The enhancement in the relaxation rate is also known as relaxivity, represented as r_1 (= $1/T_1$[CA]) and r_2 (= $1/T_2$[CA]).[10–13]

The most commonly employed T_1 CAs are Gd^{3+}-based chelates because Gd^{3+} strongly shortens T_1 due to its seven unpaired electrons and long electronic relaxation time (10^{-9} s).[13,20] These complexes show their suitable r_1-relaxivity at clinical magnetic field strengths (1.5–3.0 T). However, much higher magnetic fields (>7 T) are used for small animal (pre-clinical) imaging as the signal-to-noise, and thus resolution, is obtained at high field strength[4,21] but smaller Gd^{3+}-based chelates tumble very fast (faster than 10^{-10} s) which drastically decreases their r_1-relaxivity at higher fields.[16] Moreover, these chelates have short circulation time due to fast renal excretion limiting further their usefulness in small-animal studies.[7,15] Usually, the short circulation time has been overcome by combining the Gd^{3+} ion with bigger proteins and polymer molecules, but the tumbling times of such complexes are still too fast (10^{-10} s) for optimal performance at higher magnetic fields.[7,11] In contrast, selected NPs with longer tumbling times can overcome the shortcomings of these Gd^{3+}-based complexes. The NPs have a high density of metal ions per unit of CA enabling MR signal shortening at lower concentrations compared to chelate that usually are used at micro-molar concentrations.[15,14]

*For correspondence

Published online: 01 October 2019

NP-based CAs can broadly be categorized into two major classes, namely iron-based and Ln^{3+}-based NPs.[14,18] Iron oxide NPs (<3 nm) have been demonstrated as a T_1 CAs owing to the low magnetic moment, while the bigger iron oxide NPs are known as T_2 CAs due their superparamagnetic (SP) nature.[15,18] Nevertheless, smaller iron oxide NPs are known to be unstable in biological media and the size uniformity is still challenging for the bigger NPs.[13,9] Additionally, SP iron oxide NPs could distort the magnetic field of the neighboring normal tissues and lead to magnetic susceptibility artifact which limits their clinical application.[28] Therefore, to improve diagnostic capabilities of MRI, the iron oxide NPs labeled with Gd^{3+}-complexes have been reported as T_1–T_2 dual-mode CAs.[3,24] Consequently, to overcome the perturbation effect of SP iron oxide,[28] manganese-loaded mesoporous silica NPs have been proposed for more accurate T_1–T_2 dual-mode imaging at clinically relevant fields.[19] Therefore, for high-field (>9.4 T) MR imaging the paramagnetic lanthanide NPs could be a potential alternative because they show saturation magnetization at high field (>30 T) as demonstrated previously.[20]

Recently, dysprosium (Dy^{3+}) ion has received much attention as a potential T_2 CA for high-magnetic-field MRI because of its high effective magnetic moment (10.6 μ_B) and short electronic relaxation time ($T_{1e} \sim 10^{-13}$ s).[20] The high effective magnetic moment of Dy^{3+} would lead to higher magnetic susceptibility per unit volume of the NPs (because one NP comprises a large number of Dy^{3+} ions) which causes greater local field perturbation and thus higher r_2-relaxivity. Moreover, the short T_{1e} of Dy^{3+} allows the Curie spin to return to thermal equilibrium before the molecule changes its position or tumbles and thus becomes an important contributor to relaxivity.[20] Aforementioned, the long T_{1e} of Gd^{3+} makes it a suitable T_1 CA and r_1-relaxivity particularly dominated by the Gd^{3+} at the surface.[14,12] The use of combined T_1/T_2-weighted MR imaging that employs the same CAs could improve cancer detection (diagnostic MRI capability) accuracy and it could be achieved by Dy^{3+} and Gd^{3+} core/shell nanostructures as shown in the proposed scheme in Figure 1.[12] However, in the current review we will discuss the capability of $NaDyF_4$ nanoparticles as T_2 CA for high field MRI diagnostic.

1.1 *Experimental design*

The synthesis of hexagonal $NaREF_4$ (RE = Dy, Gd, Y) can be carried out with their RE (III) acetate hydrate or with RE(III) chloride hydrate. In a typical synthesis of 1 mmol of $NaDyF_4$, 0.78 mmol of dysprosium (III) chloride hydrates were added to 50 mL three-neck round bottom flask subsequently, added 1.5 mL oleic acid together with 7.5 mL of 1-octadecene.[1] Consequently, the mixtures were heated under vacuum to 140 °C with continuous stirring for 30 min that produces the dysprosium-oleates complex. The complex mixture was cool down to room temperature. Subsequently, added the 2.8 mmol of NaOH and 4 mmol of NH_4F dissolved in 7.5 mL of methanol that precipitated the complex. Later, the precipitates were mixed together at room temperature (25 °C) that gave the homogenous solution mixture. Then the temperature of the solution mixture was slowly raised to 65 °C to remove the methanol and other impurities such as chlorides from the solution mixture. After the removal of the impurities, the temperature of the solution mixture was raised to ~300 °C at the rate ~15 to 20 °C per minutes for 1.5 h in an inert gas atmosphere. Subsequently, the mixture was cool down to room temperature and precipitated with an excess of ethanol and washed out by centrifugation. The obtained product was hexagonal oleate-stabilized $NaREF_4$ nanoparticles. The sizes of these nanoparticles can be tuned with respect to reaction time. The nanoparticles synthesized up to this stage (assume stage I) would act as either T_1 or T_2 contrast agent, because the synthesized product would be $NaGdF_4$ or $NaDyF_4$ i.e., only the core nanoparticles.

In case of the materials, needed for both T_1–T_2 diagnostic simultaneously, at stage I, the pre-synthesized calculated amount of sacrificial, cubic $NaGdF_4$ nanoparticles would be injected and after the completion of the reaction the product would be oleate-stabilized $NaDyF_4$/$NaGdF_4$ nanoparticles. The synthesis of cubic nanoparticles has been reported.[1]

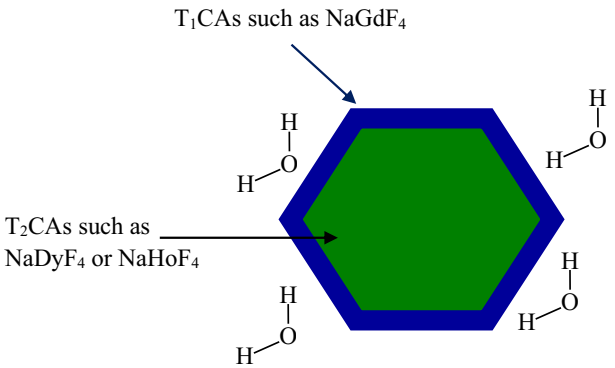

Figure 1. Schematic representation of the model for T_1–T_2 MRI diagnostic simultaneously.

However, as we mentioned earlier the plan in this review is to discuss more about $NaDyF_4$ nanoparticles that are a potent T_2 MRI contrast agent. The desired $NaDyF_4$ nanoparticles of any size can be achieved adjusting reaction time. Their syntheses are very similar as proposed in the scheme in Figure 2. For instance, different sizes of nanoparticles 5.4 nm, 9.8 nm, and 20.3 nm have been reported (Figure 3);[10] their shapes were nearly spherical as shown in Figure 4. The surface modifications of these oleate-stabilized $NaDyF_4$ nanoparticles were performed with amphiphilic poly(maleic anhydride-*alt*-1-octadecene) (PMAO) and poly(ethylene glycol) methyl ether (PEG-OH) using chloroform as a solvent. After the

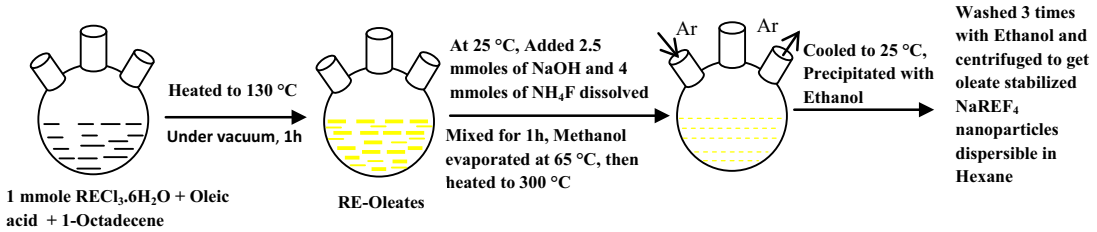

Figure 2. Schematic representation of the synthesis process of $NaREF_4$ nanoparticles.

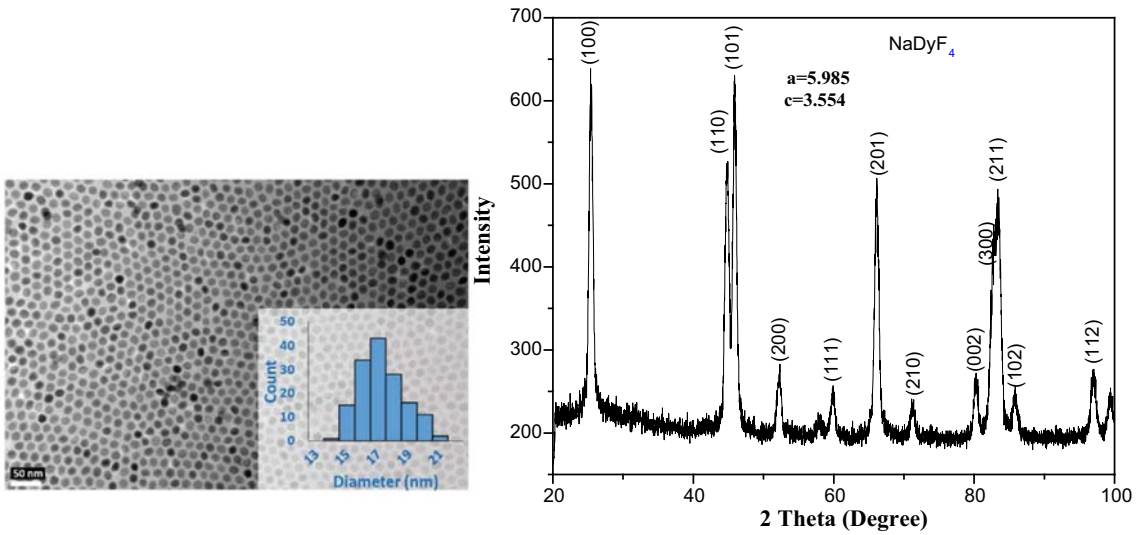

Figure 3. (**a**) The TEM image and (**b**) XRD of synthesized $NaDyF_4$ nanoparticles. This figure is reprinted with permission from Ref.[1] Copyright (2017) American Chemical Society.

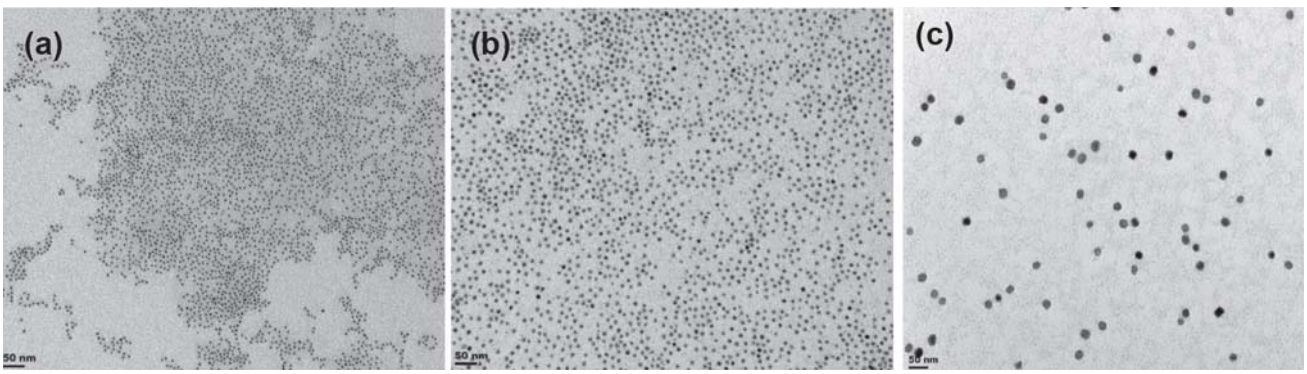

Figure 4. TEM image of $NaDyF_4$ nanoparticles (**a**) 5.4 nm, (**b**) 9.8 nm and (**c**) 20.3 nm. This figure is reprinted with permission from Ref.[10] Copyright (2011) American Chemical Society.

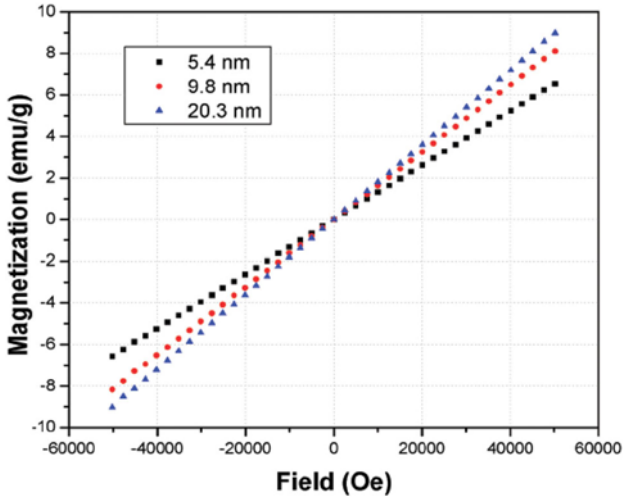

Figure 5. SQUID magnetometer data of mass magnetize $NaDyF_4$ nanoparticles. This figure is reprinted with permission from Ref.[10] Copyright (2011) American Chemical Society.

evaporation of the chloroform, the water dispersible PMAO-PEG modified nanoparticles were obtained.[10]

The SQUID magnetometer of $NaDyF_4$ nanoparticles of sizes 5.4, 9.8 and 20.3 nm has been reported by Gautom *et al*.[10] shown in Figure 5. It is clear from Figure 5 that magnetization of nanoparticles increases with the increase in the size of the particles. The reasons of increase in the magnetization of the bigger nanoparticles were due to the availability of a greater number of Dy^{3+} compared to their availability in the smaller nanoparticles. Usually, the overall magnetization of the nanoparticles remained independent of the shape for $NaDyF_4$ nanoparticles as reported by Zhang *et al*.[27] For instance, as shown in Figure 6, the measured magnetization of rod-like $NaDyF_4$ nanoparticles of dimension (15 nm × 20 nm) was nearly 7 emu/g, however as the dimension changes to (19 nm × 25 nm) the magnetization changed to 8 emu/g at 7 Oersted.[27] Furthermore, as the size of nanoparticles increases to 25 nm × 35 nm, the magnetization increases to 10.8 emu/g at the same magnetic field.[27] The surfaces of these oleate-stabilized (hydrophobic in nature) nanoparticles were further modified with PMAO-PEG in order to disperse in water.[10,27]

1.2 *Relaxivity measurement of the PMAP-PEG coated $NaDyF_4$ nanoparticles*

Relaxivity of a CA can be defined as a change in the relaxation rate after addition of a CA, normalized to

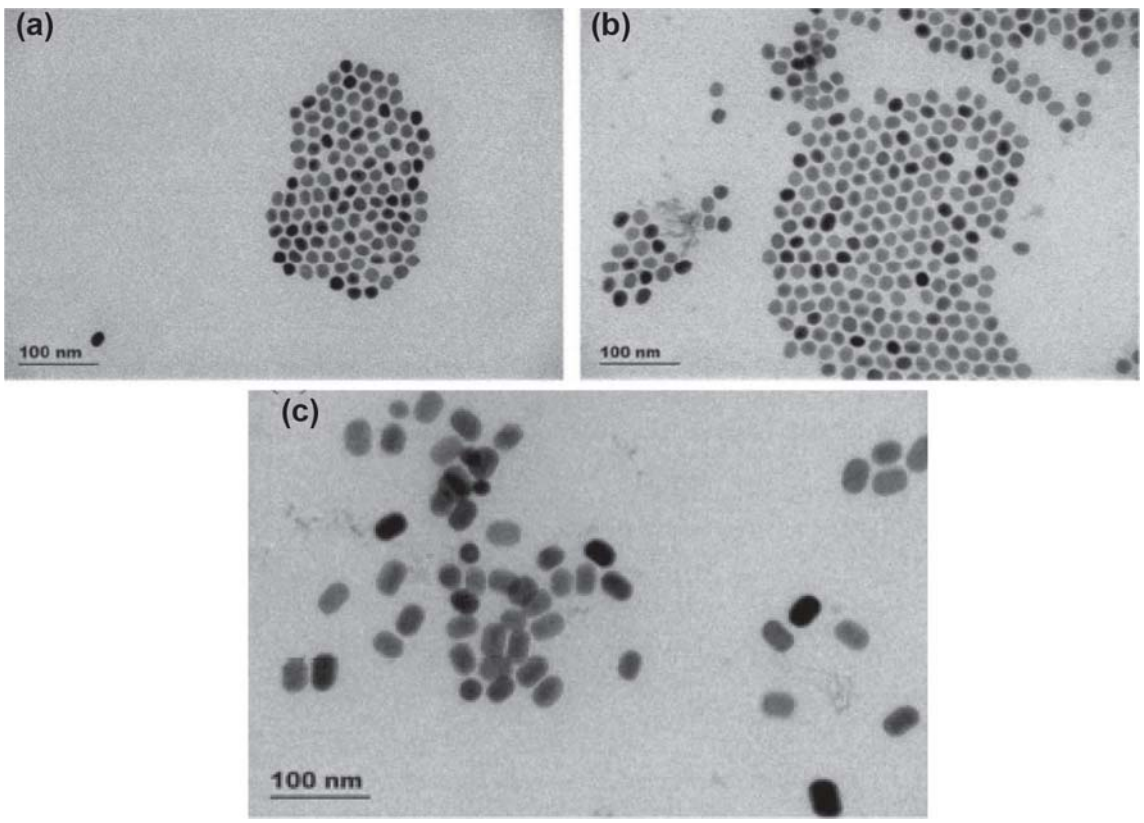

Figure 6. TEM image of $NaDyF_4$ nanoparticles of sizes (**a**) 15 nm × 20 nm, (**b**) 19 nm × 25 nm and (**c**) 25 nm × 35 nm. This figure is reprinted with permission from Ref.[27] Copyright (2016) American Chemical Society.

Table 1. r_2-relaxivities of $NaDyF_4$ nanoparticles and 9.4 T.

9.4 T						
Contrast agents	Size (nm)	Shape	$r_2[Dy^{3+}]$ (mM^{-1} s^{-1})	per NPs (mM^{-1} s^{-1})	Surface coating	References
$NaDyF_4$	5.4	Spherical	32	50×10^4	PMAO-PEG	10
$NaDyF_4$	9.8	Spherical	51	350×10^4	PMAO-PEG	10
$NaDyF_4$	20.3	Spherical	101	570×10^4	PMAO-PEG	10
$NaDyF_4$	15 × 20	Elongated	65	313×10^4	PMAO-PEG	27
$NaDyF_4$	19 × 25	Elongated	91	1117×10^4	PMAO-PEG	27
$NaDyF_4$	25 × 35	Elongated	204	4767×10^4	PMAO-PEG	27

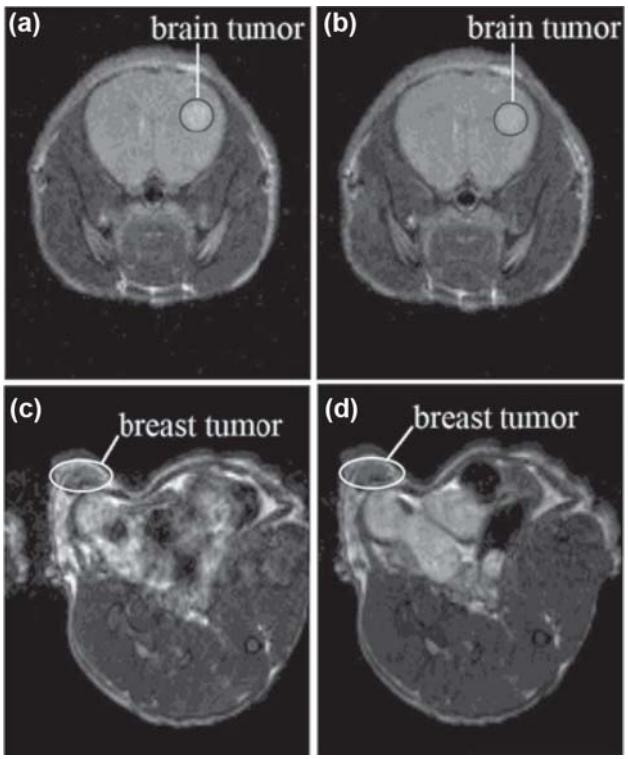

Figure 7. *In vivo* T_2-weighted MR images of tumor bearing mice: brain tumor and breast tumor before (left) and 12 min post injection (right) of the $NaDyF_4$ nanoparticles. This figure is reprinted with permission from Ref.[27] Copyright (2016) American Chemical Society.

the concentration of the CA. The equation is given below,[6,12]

$$r_i = \Delta(1/T_i)/[M],$$

where i = 1 or 2, and M is the concentration of CA.

As we mentioned the $NaDyF_4$ is T_2 contrast agent, therefore for the Dy^{3+}-based nanoparticles (i = 2) then

$$r_2 = \Delta(1/T_2)/[M],$$

The relaxivity is usually governed by the in-sphere and outer-sphere mechanism for lanthanide-based complexes.[12] However, due to the hydrophobic barrier on the surface of nanoparticles, the water molecules get prohibited to reach the surface of the metal nanoparticles. Therefore, the only out-sphere contribution is expected that will lead to r_2-relaxivity (Table 1).

Zhang *et al.*[27] achieved the highest r_2-relaxivity 204 mM^{-1} s^{-1} per Dy^{3+} with the 25 nm × 35 nm, elongated $NaDyF_4$ nanoparticles. Therefore, it was more appropriate for MRI at high field (9.4 T) and used for MR imaging of the brain tumor and breast tumor of mice. These nanoparticles were injected into mice via the tail vein. The amount of nanoparticles injected was 0.25 mL of NaDyF4 (25 nm × 35 nm) in water weighing 2 mg/mL of $NaDyF_4$. The MR images are shown in Figure 7. Figure 7a shows the brain tumor (high-grade glioma) bearing the image before injection of nanoparticles. Figure 7b shows the brain tumor (high-grade glioma) bearing image 12 min post injection of the $NaDyF_4$ nanoparticles. The contrasts between the tumor and brain tissue are evidently seen in Figure 7a and 7b. The increased T_2 contrast can be seen in Figure 7b, due to the accumulation of $NaDyF_4$ nanoparticles at the tumor site. The similar effects were also seen in breast tumor Figure 7c and 7d before and after injection respectively. The maximum T_2 reduction was 13.5% just after the injection of the $NaDyF_4$ nanoparticles. The result suggested that $NaDyF_4$ nanoparticles were effective in the detection of both brain and breast tumors.[27]

2. Conclusions

In this article, we have discussed why there is need of a relevant CA for a high magnetic field application. Additionally, we discussed the advantages of $NaREF_4$ nanoparticles over the RE-based complexes (RE = Gd, Dy) as an MRI CA. Moreover, we have compared the SQUID magnetometer data of $NaDyF_4$ nanoparticles of different size and shapes. The result suggested that magnetization was independent of the shape for $NaDyF_4$ nanoparticles. However, the magnetization of nanoparticles increases with the increasing particles size. The reason of increase in the

magnetization of the bigger nanoparticles was due to the availability of a greater number of Dy^{3+} compared to their availability in the smaller nanoparticles. Finally, the biggest size i.e., 25 nm × 35 nm elongated $NaDyF_4$ nanoparticles were used for the MRI of brain and breast tumors at 9.4 T had shown good contrast between normal brain tissue and the tumor region. The result suggested the $NaDyF_4$ nanoparticles have the potential for high field MRI applications as T_2 CA.

References

1. Alvares R D A, Gautam A, Prosser R S, van Veggel F C J M and Macdonald P M 2017 Shell versus core Dy^{3+} contributions to NMR water relaxation in sodium lanthanide fluoride core-shell nanoparticles. An investigation using O-17 and H-1 NMR *J. Phys. Chem. C* **121** 17552
2. Arya S K and Bhansali S 2011 Lung cancer and its early detection using biomarker-based biosensors. *Chem. Rev.* **111** 6783
3. Bae K H, Kim Y B, Lee Y, Hwang J, Park H and Park T G 2010 Bioinspired synthesis and characterization of gadolinium-labeled magnetite nanoparticles for dual contrast T_1- and T_2-weighted magnetic resonance imaging *Bioconjugate Chem.* **21** 505
4. Bokacheva L, Ackerstaff E, LeKaye H C, Zakian K and Koutcher J A 2014 High-field small animal magnetic resonance oncology studies *Phys. Med. Biol.* **59** R65
5. Cao C, Wang X, Cai Y, Sun L, Tian L, Wu H, He X, Lei H, Liu W, Chen G, Zhu R and Pan Y 2014 Targeted in vivo imaging of microscopic tumors with ferritin-based nanoprobes across biological barriers *Adv. Mater.* **26** 2566
6. Caravan P, Ellison J J, McMurry T J and Lauffer R B 1999 Gadolinium(III) chelates as MRI contrast agents: structure, dynamics, and applications *Chem. Rev.* **99** 2293
7. Caravan P, Farrar C T, Frullano L and Uppal R 2009 Influence of molecular parameters and increasing magnetic field strength on relaxivity of gadolinium- and manganese-based T1 contrast agents *Contrast Media Mol. Imaging* **4** 89
8. Chen S, Wang L, Duce S L, Brown S, Lee S, Melzer A, Cuschieri S A and André P 2010 Engineered biocompatible nanoparticles for *in vivo* imaging applications *J. Am. Chem. Soc.* **132** 15022
9. Coey J M D 1971 Noncollinear spin arrangement in ultrafine ferrimagnetic crystallites *Phys. Rev. Lett.* **27** 1140
10. Das G K, Johnson N J J, Cramen J, Blasiak B, Latta P, Tomanek, B and van Veggel F C J M 2012 $NaDyF_4$ Nanoparticles as T2 contrast agents for ultra-high field magnetic resonance imaging *J. Phys. Chem. Lett.* **3** 524
11. Debroye E and Parac Vogt T N 2014 Towards polymetallic lanthanide complexes as dual contrast agents for magnetic resonance and optical imaging *Chem. Soc. Rev.* **43** 8178
12. Gautam A and Komal P 2018 Probable ideal size of Ln^{3+}-based upconversion nanoparticles for single and multimodal imaging *Coord. Chem. Rev.* **376** 393
13. Gautam A and van Veggel F C J M 2013 Synthesis of nanoparticles, their biocompatibility, and toxicity behavior for biomedical applications *J. Mater. Chem. B* **1** 5186
14. Johnson N J J, Oakden W, Stanisz G J, Scott Prosser R and van Veggel F C J M 2011 Size-tunable, ultrasmall $NaGdF_4$ nanoparticles: Insights into their T_1 MRI contrast enhancement *Chem. Mater.* **23** 3714
15. Kim B H, Lee N, Kim H, An K, Park Y I, Choi Y, Shin K, Lee Y, Kwon S G, Na H B, Park J G, Ahn T Y, Kim Y W, Moon W K, Choi S H and Hyeon T 2011 Large-scale synthesis of uniform and extremely small-sized iron oxide nanoparticles for high-resolution T_1 magnetic resonance imaging Contrast Agents *J. Am. Chem. Soc.* **133** 12624
16. Lee G Y, Qian W P, Wang L, Wang Y A, Staley C A, Satpathy M, Nie S, Mao H and Yang L 2013 Theranostic nanoparticles with controlled release of gemcitabine for targeted therapy and MRI of pancreatic cancer *ACS Nano* **7** 2078
17. Mahmoudi M, Hosseinkhani H, Hosseinkhani M, Boutry S, Simchi A, Journeay W S, Subramani K and Laurent S 2011 Magnetic resonance imaging tracking of stem cells in vivo using iron oxide nanoparticles as a tool for the advancement of clinical regenerative medicine *Chem. Rev.* **111** 253
18. Na H B, Song I C and Hyeon T 2009 Inorganic nanoparticles for MRI contrast agents *Adv. Mater.* **21** 2133
19. Niu D, Luo X, Li Y, Liu X, Wang X and Shi J 2013 Manganese-loaded dual-mesoporous silica spheres for efficient T1- and T2-weighted dual mode magnetic resonance imaging *ACS Appl. Mater. Interfaces* **5** 9942
20. Norek M and Peters J A 2011 MRI Contrast agents based on dysprosium or holmium *Progr. Nucl. Magn. Reson. Spectrosc.* **59** 64
21. Ooi Y, Inui Yamamoto C, Suzuki T, Nakadate H, Nagase Y, Seiyama A, Yoshioka Y and Seki J 2014 In vivo magnetic resonance imaging at 11.7 tesla visualized the effects of neonatal transection of infraorbital nerve upon primary and secondary trigeminal pathways in rats *Brain Res.* **1579** 84
22. Seo W S, Lee J H, Sun X, Suzuki Y, Mann D, Liu Z, Terashima M, Yang P C, McConnell M V, Nishimura D G and Dai H 2006 FeCo/graphitic-shell nanocrystals as advanced magnetic-resonance-imaging and near-infrared agents *Nat. Mater.* **5** 971
23. Wu M, Meng Q, Chen Y, Xu P, Zhang S, Li Y, Zhang L, Wang M, Yao H and Shi J 2014 Ultrasmall confined iron oxide nanoparticle MSNs as a pH-responsive theranostic platform *Adv. Funct. Mater.* **24** 4273
24. Yang H, Zhuang Y, Sun Y, Dai A, Shi X, Wu D, Li F, Hu H and Yang S 2011 Targeted dual-contrast T1- and T2-weighted magnetic resonance imaging of tumors using multifunctional gadolinium-labeled superparamagnetic iron oxide nanoparticles *Biomaterials* **32** 4584
25. Yeh C S, Su C H, Ho W Y, Huang C C, Chang J C, Chien Y H, Hung S T, Liau M C and Ho H Y 2013 Tumor targeting and MR imaging with lipophilic

cyanine-mediated near-infrared responsive porous Gd silicate nanoparticles *Biomaterials* **34** 5677
26. Yoo D, Lee J H, Shin T H and Cheon J 2011 Theranostic magnetic nanoparticles *Acc. Chem. Res.* **44** 863
27. Zhang X, Blasiak B, Marenco A J, Trudel S, Tomanek B and van Veggel F C J M 2016 Design and regulation of $NaHoF_4$ and $NaDyF_4$ nanoparticles for high-field magnetic resonance imaging *Chem. Mater.* **28** 3060
28. Zhou Z, Huang D, Bao J, Chen Q, Liu G, Chen Z, Chen X and Gao J A 2012 Synergistically enhanced T_1–T_2 dual-modal contrast agent *Adv. Mater.* **24** 6223